BJCP British Journal of Clinical Pharmacology

DOI:10.1111/j.1365-2125.2008.03109.x

Population pharmacokinetic modelling for enterohepatic circulation of mycophenolic acid in healthy Chinese and the influence of polymorphisms in UGT1A9

Zheng Jiao,[1,2] Jun-jie Ding,[3] Jie Shen,[4] Hui-qi Liang,[2] Long-jin Zhong,[2] Yi Wang,[2] Ming-kang Zhong[2] & Wei-yue Lu[1]

[1]School of Pharmacy, [2]Clinical Pharmacy Laboratory, Huashan Hospital, [3]Department of Pharmacy, The Children's Hospital and [4]Department of Pharmacy, Huadong Hospital, Fudan University, Shanghai, China

Correspondence
Professor Wei-yue Lu, School of Pharmacy, Fudan University, 138 Yi Xue Yuan Raod, Shanghai 200032, China.
Tel: + 86 21 5423 7040
Fax: + 86 21 5423 7040
E-mail: wylu@shmu.edu.cn

Keywords
enterohepatic circulation, mycophenolic acid, population pharmacokinetics, UGT1A9

Received
22 March 2007

Accepted
21 December 2007

Published *OnlineEarly*
15 February 2008

WHAT IS ALREADY KNOWN ABOUT THIS SUBJECT

- Mycophenolic acid (MPA) undergoes enterohepatic circulation (EHC) in the body and several population models have been proposed to describe this process using sparse data.
- Recent studies in Whites have found that polymorphism in UGT1A9 could partly explain the large interindividual variability associated with the pharmacokinetics of MPA.

WHAT THIS STUDY ADDS

- A new population pharmacokinetic model for EHC combining MPA and its main glucuronide metabolite (MPAG) simultaneously was established based on physiological aspects of biliary excretion using intensive sampling data.
- Pharmacokinetic profiles of MPA and MPAG with the UGT1A9 polymorphism in healthy Chinese were characterized.

AIMS

To establish a population pharmacokinetic model that describes enterohepatic circulation (EHC) of mycophenolic acid (MPA) based on physiological considerations and to investigate the influence of polymorphisms of UGT1A9 on the pharmacokinetics of MPA.

METHODS

Pharmacokinetic data were obtained from two comparative bioavailability studies of oral mycophenolic mofetil formulations. Nonlinear mixed effects modelling was employed to develop an EHC model including both MPA and its main glucuronide metabolite (MPAG) simultaneously. Demographic characteristics and UGT1A9 polymorphisms were screened as covariates.

RESULTS

In total, 590 MPA and 589 MPAG concentration–time points from 42 healthy male volunteers were employed in this study. The chain compartment model included an intestinal compartment, a gallbladder compartment, a central and a peripheral compartment for MPA and a central compartment for MPAG. The typical population clearance (CL/*F*) estimates with its relative standard error for MPA and MPAG were 10.2 l h^{-1} (5.7%) and 1.38 l h^{-1} (6.9%), respectively. The amount of MPA recycled in the body was estimated to be 29.1% of the total amount absorbed. Covariate analysis showed that body weight was positively correlated with CL/*F* of MPA, intercompartment CL/*F* of MPA and distribution volume of MPA peripheral compartment. Polymorphisms of UGT1A9 did not show any effect on the pharmacokinetics of MPA and MPAG. The model evaluation tests indicated that the proposed model can describe the pharmacokinetic profiles of MPA and MPAG in healthy Chinese subjects.

CONCLUSIONS

The proposed model may provide a valuable approach for planning future pharmacokinetic–pharmacodynamic studies and for designing proper dosage regimens of MPA.

Introduction

Mycophenolate mofetil (MMF), a prodrug of the immunosuppressive agent mycophenolic acid (MPA), is widely used in immunosuppressive regimens with corticosteroids and calcineurin inhibitors for the prophylaxis of rejection in solid organ transplantation [1–3]. After oral administration, MMF undergoes rapid and complete hydrolysis to MPA. MPA has extensive plasma albumin binding (>97%) and is metabolized by uridine glucuronosyl transferase (UGT) enzymes into the pharmacologically inactive metabolite mycophenolic acid 7-O-glucuronide (MPAG) [4]. The pharmacokinetics (PK) of MPA is characterized further by enterohepatic circulation (EHC), in which MPAG is excreted into bile and rehydrolysed to MPA in the intestine and reabsorbed as MPA. The EHC of MPA has been estimated to be approximately 40%, with a range of 10–60% [4].

Conventional PK models are inappropriate for such data and can not define multiple peaks and the magnitude of EHC. Several models have been proposed to describe EHC profiles of MPA using a population approach [5–8]. However, in these previous studies sparse data were employed to build the model, which could lead to an unidentifiable model structure and inappropriate characterization of the EHC process [9–11]. Lack of fit in the elimination phase and failure to identify multiple peaks have been observed [5–7]. Our group once established an EHC model using more intensive sampling data from 20 subjects [8]. The established model could well define the second peak as well as area under the concentration–time curve (AUC). However, EHC was modelled as a continuous process, not discrete biliary excretion episodes, which is inconsistent with the physiological process [12]. Moreover, MPAG, which has no pharmacological activity but plays an important role in the EHC process, was not incorporated into the model, nor has it been incorporated in most of the above-mentioned studies. Lack of such information in the modelling can lead to incomplete and biased understanding of the PK of MPA. Therefore, the first aim of the current study was to establish an EHC model that combines MPA and MPAG simultaneously based on physiological aspects of biliary excretion using intensive sampling data.

Clinical MPA PK is characterized by large interindividual variability [13–15]. The genetic factors controlling the level of UGT-mediated MPA metabolism explain in part the variability in MPA exposure [16–20]. UGT1A9 is the most important UGT isoform involved in glucuronidation of MPA, accounting for >50% of MPAG production in the liver, kidney and intestinal mucosa [16, 18]. Yamanaka H *et al.* [21] have reported that a base insertion T_{10} from −109 to −98 in the promoter region could increase reporter gene expression in HepG2 cells and may alter the level of enzyme expression. Girard H *et al.* [17] have confirmed the presence of this single nucleotide polymorphism (SNP), but found no association with changes in UGT1A9 protein levels. They demonstrated another 10 SNPs in the UGT1A9 promoter region. In human liver microsomes, they proved that UGT1A9 expression varied by 17-fold and was significantly correlated with SNPs of −275, −331/−440, −665 and −2152. Recently, Kuypers *et al.* [22] have observed that the −275T/A and −2152C/T SNPs were associated with significantly lower MPA exposure in White renal transplant recipients treated with MMF. The allele frequencies of UGT1A9 −275T/A and −2152C/T SNPs in Whites are reported to be 16.8% and 12.6%, whereas these polymorphisms are not found in Japanese [23, 24]. Moreover, Girard *et al.* [17] have also found that the glucuronosyltransferase activity for MPA was lower in one individual carrying the UGT1A9*3 allele (+98T/C), indicating decreased enzymatic activity caused by this mutation in the coding region (codon 33) of the *UGT1A9* gene. Since little is known in the Chinese population, the second aim of this study was to genotype the SNPs of UGT1A9 previously reported and investigate their effects on the PK of MPA in Chinese using the proposed population EHC model.

Materials and methods

Drugs and reagents

MPA was obtained from Fluka Chemie (Buchs, Switzerland) and MPAG was produced by Analytical Services International Ltd (London, UK). Both standards were of >98% purity. The internal standard propafenone was obtained from Shanghai Institute for Drug Control. Trifluoroacetic acid (TFA) was purchased from Shanghai Chemicals and Reagents Ltd. High-performance liquid chromatography (HPLC)-grade methanol and acetonitrile were purchased from Burdick & Jackson Honeywell International Inc. (Muskegon, MI, USA). The water was filtered through the Millipore Milli-Q system (Milford, MA, USA). MMF capsules of 0.25 g (Cellcept®) were manufactured by Shanghai Roche Ltd, China. All other chemicals and solvents used were of analytical grade.

Study protocol

Plasma concentration data for PK modelling were obtained from two bioequivalence studies which employed standard open-label, single-dose, randomized crossover design, with a wash-out period of 12 days separating the dosing periods. The study protocols were approved by the independent Clinical Research Ethics Committee of Huashan Hospital, Fudan University. Written informed consent was obtained from each subject prior to enrolment in the study.

Twenty and 22 healthy Chinese volunteers were enrolled in the first and second studies, respectively. All subjects underwent a physical examination, ECG evaluation, haematological and blood chemistry test, and a thorough medical history review to ensure that they were healthy. Participants were excluded if they had a history of biliary tract disease, biliary tract surgery, or gastrointestinal

surgery. Consumption of alcohol was prohibited from 72 h before the first dose of MMF until the end of the study; consumption of caffeine was prohibited from 12 h before each dose of study medication until 12 h after each dose.

During each of the treatment periods, participants fasted overnight for at least 10 h with access to water only. Each participant then received 0.5 g of MMF given as either two 0.25-g test or two 0.25-g reference formulations with 200 ml of water. Fasting continued until 4 h after the start of drug administration, at which time a standard lunch was served. Standardized meals were given 10, 24.25 h and 9.5, 24.25 h after drug administration in the first and second studies, respectively. Blood samples were collected predose and at 0.25, 0.5, 0.75, 1, 1.5, 2, 3, 4, 6, 8, 12, 24, 36 and 48 h postdose in the first study and predose, 0.17, 0.33, 0.5, 0.75, 1, 2, 3, 4, 5, 6, 8, 10, 12, 24, 36 and 48 h postdose in the second study. All blood samples were centrifuged within 30 min after collection for 15 min at 3000 *g* and 4°C. The plasma was separated, transferred into clean polypropylene tubes and stored frozen at −20°C until analysis.

Since the focus of this study was not to discuss bioequivalence issues regarding the formulations investigated but the EHC profile of MPA, only concentration–time data obtained following administration of the Cellcept® formulation were used.

Determination of plasma levels of MPA and MPAG

MPA and MPAG plasma concentrations were determined by a validated HPLC method, with small modifications [25]. Briefly, the analytes were extracted by a protein precipitation process, which employed 200 µl of acetonitrile containing the internal standard propafenone (150 mg l^{-1}), as the protein precipitant reagent. The separations were carried out using a Kromasil C_8 analytical column (150 × 4.6 mm, 5 µm; AKZONOBEL, Bohus, Sweden) with the isocratic elution system of methanol and water containing 0.1% TFA (54 : 46, v/v). MPAG was determined by ultraviolet detection at 250 nm, whereas MPA was quantified by fluorescence detection after postcolumn online derivation of 0.2 M sodium hydroxide solution. The excitation and emission wavelengths were set at 325 nm and 435 nm, respectively. The method was found to be linear over the concentration range investigated, 0.1–40 mg l^{-1} and 2.5–200 mg l^{-1} for MPA and MPAG, respectively. Both the coefficient variations of intraday and interday were <12% and bias from the nominal value was <8.3%.

Identification of genotypes

Genomic DNA was extracted from ethylenediamine tetraaceticacid-treated whole blood by a SilMax™ Plasmid DNA Miniprep Kit (SBS Genetech Corp., Beijing, China). Genotyping was performed by independent external contractors (UGT1A9 promoter: Shanghai GeneCore BioTechnologies Co. Ltd, Shanghai, China; UGT1A9*3: Shanghai Biowing Applied Biotechnology Co. Ltd, Shanghai, China). Hardy–Weinberg equilibrium testing was performed using appropriate χ^2 testing by the software SHEsis [26].

Polymerase chain reaction (PCR) was used to amplify the UGT1A9 promoter region from −2224 to +2 (relative to the translational start site). Total volume for each reaction was 25 µl, including template 5–10 ng, Taq enzyme 0.125 U, $MgCl_2$ 1.5 µl (25 mM), dNTP 2 µl (25 mM), 10× buffer 2.5 µl and primers 0.5 µl each (20 µM) (TaKaRa Biotechnology Co., Ltd, Dalian, China). The sequence of the two pairs of forward (F) and reverse (R) primers was as follows: F1 (TTT TCA ATT GTT CAT TGC TA) and R1 (CTA CTC AAT GGA GGA CAA TC) for the mutations of −2208C/T, −2152C/T, −2141C/T, −1887T/G and −1818T/C; F2 (AGC AGA CTG AGA GAG ACA AG) and R2 (CAG ACA CAC ACA TAG AGG AA) for the mutations of −665C/T, −440T/C, −331C/T, −275T/A, −87G/A and −109 to −98 base pair (bp) insertion, respectively. The amplification products were 664 and 680 bp, respectively. After 2 min incubation at 98°C, amplification was performed first for 11 cycles at 96°C 30 s, 60°C 1 min (decrease 1°C for each cycle), 72°C 45 s, then PCR conditions were changed to 96°C 30 s, 55°C 40 s, 72°C 45 s, for another 35 cycles. The reaction was completed by 7 min extension at 72°C. PCR products were purified on Qiagen quick columns (Qiagen Inc., Mississauga, ON, Canada) and sequenced with primers using an ABI PRISM 3700 DNA Analyser (Applied Biosystem, Foster City, CA, USA). All sequences were analysed with the Staden preGap4 and Gap4 programs. Ambiguous sequencing chromatograms and samples with SNPs were systematically reamplified and resequenced.

UGT1A9*3 (+98T/C) polymorphisms were determined by using PCR-restriction fragment length polymorphism procedures as previously described [22]. Samples (20 µl) were of a PCR mixture containing 100 ng of genomic DNA template, 1.5 mM $MgCl_2$, 0.5 µmol of forward primer (5′-GTT CTC TGA TGG CTT GCA CA-3′) and reverse primer (5′-ATG CCC CCT GAG AAT GAG TT-3′), 200 µM dNTP mixture, and 1 U of polymerase (Promega Biotech Co., Ltd, Madison, WI, USA). Amplification was performed with a Perkin Elmer 9600 Thermal Cycler (PerkinElmer Life and Analytical Sciences, Inc., Waltham, MA, USA). The PCR amplification conditions were as follows: 2 min at 95°C; 35 cycles of 30 s at 94°C, 35 s at 60°C, and 30 s at 72°C; and finally, 6 min at 72°C The PCR product was digested by 10 U of restriction enzyme *Sty*I and then processed by electrophoresis on a 3% agarose gel.

Model development

Data were analysed by the population PK package NONMEM (version 6.1; Icon Inc., North Wales, PA, USA) in conjunction with a G77 FORTRAN compiler. Post processing of NONMEM output was undertaken with Xpose (Version 4.0 preview, release 6) [27], programmed in the statistics package R (version 2.3.1). As models using conditional estimation algorithm had extremely long run times and failed to converge, the first order estimation (FO) algorithm was employed in the model-building process. At the

final step FO with η–ε interaction (FO-I), the first-order conditional estimation with or without η–ε interaction algorithm (FOCE or FOCE-I) were tried to obtain more accurate parameter estimates [28, 29]. When the FOCE method was employed, conditional weighted residuals were calculated [30]. Data with or without natural logarithm transformation were also tested. To develop a metabolite PK model, MMF doses, MPA and MPAG plasma concentrations were converted to molar equivalents. As the use of 'mg l^{-1}' is widely recognized by physicians and pharmacologists, the data were recalculated in the figures and results. Moreover, for clinical relevance the PK model was parameterized in terms of apparent clearance (CL/*F*) and volume of distribution (*V*/*F*) where possible.

Before parameter estimation, structural identifiability analysis was performed to assure proposed model parameters could be practically determined. Structural identifiability analysis was performed by use of the similarity transformation approach [11]. Matrix calculation was performed with the symbolic calculation software Mathematica (Version 4.0; Wolfram Research Inc., Champaign, IL, USA). Based on the results of identifiability analysis, the integrated solutions for the plasma concentrations of MPA and MPAG were subsequently obtained.

Model selection was based on goodness-of-fit [31] in addition to the three commonly used criteria of statistical significance, plausibility and stability. Models were compared statistically using a likelihood ratio test on the differences in the objective function value (OFV). Statistical significance was set at $P < 0.01$. Plots of residuals and weighted residuals, standard errors of parameter estimates and changes in estimates of interindividual and residual variability were also examined. PK parameter estimates were required to be physiologically plausible. A model had to remain stable when significant digits and initial parameter estimates were altered.

Preliminary analysis focused on selection of a structural model. Based on physiological considerations, the basic structural model included a gastrointestinal (GI) compartment, a MPA central compartment, a MPAG central compartment and a gallbladder (GB) compartment. The MMF dose was entered into the GI compartment and the EHC process was modelled by introducing a rate constant describing transfer from the MPAG central compartment to the GB compartment. When GB emptying occurred, MPAG was reintroduced to the GI compartment and converted to MPA, followed by reabsorption into the central compartment of MPA. Peripheral compartments for MPA, MPAG or both were tested. Zero and first-order absorption with or without lag time were also examined.

Exponential models were used to account for interindividual variability and all parameters were tested initially. The value of a parameter in an individual (P_i) is a function of the parameter value in the typical individual ($\acute{P}$) and an individual deviation represented by η_i. The η_is in the population are symmetrically distributed, zero-mean random variables with a variance that is estimated as part of the model estimation from Equation 1:

$$P_i = \acute{P} \times \exp(\eta_i) \quad (1)$$

Various statistical models describing the random residual variability were considered:

$$Y = IPRED + \varepsilon \quad (2)$$

$$Y = IPRED \times \exp(\varepsilon) \quad (3)$$

$$Y = IPRED \times \exp(\varepsilon_1) + \varepsilon_2 \quad (4)$$

where *Y* represents the observation, *IPRED* is the individual predicted concentration and ε_n is symmetrically distributed, zero-mean random variables with variance terms that are estimated as part of the population model-fitting process.

The covariates effects were tested on all PK parameters, which included age, height, body weight, serum creatinine, serum albumin, haemoglobin, creatinine clearance and UGT1A9 polymorphisms. Creatinine clearance was calculated from serum creatinine values using the standard Cockcroft and Gault equation [32]. Generalized additive modelling (GAM) [33], implemented in Xpose, was used to identify possibly influential variables. Covariates identified in the GAM as being important were included in the mixed-effects model applying a stepwise procedure. Each covariate was incorporated stepwise into the basic regression model. A difference in the OFVs of >3.84 (χ^2-value associated with $P < 0.05$ for one degree of freedom) was required to indicate that the model with the lowest OFV was probably better than the previous one. Improvement was also sought in plots obtained from the more complex model relative to the basic one. This process was continued until no further reduction in the OFV resulted. Finally, a backwards elimination step was performed by setting the coefficient of each covariate, in turn, to zero and noting the change in OFV. To partially compensate for the multiple comparisons, a more restrictive criterion was adopted and a difference in the OFVs of >6.63 ($P < 0.01$) was required to maintain the factor in the model.

Covariate relationships were modelled proportional to the parameter, as the fractional change in the parameter with the covariate. Covariates that were continuous variables were centred to their median values in a linear (Equations 5 and 6) or nonlinear (Equation 7) manner so that the population estimates would represent those of an average subject, for example:

$$CL/F = \theta_1 \times \left(\frac{WT_i}{WT_m}\right) \quad (5)$$

$$CL/F = \theta_1 + \theta_2 \times (WT_i - WT_m) \quad (6)$$

$$CL/F = \theta_1 \times \left(\frac{WT_i}{WT_m}\right)^{\theta_2} \quad (7)$$

where WT_i is the body weight of the i*th* individual, and WT_m represents median body weight. For the categorical covariates, such as UGT1A9 SNPs, a change in the CL/*F* of MPA was evaluated by the following equation:

$$CL/F = \begin{cases} \theta_1 & \text{if homozygous wild-type carriers} \\ \theta_1 \cdot \theta_2 & \text{if heterozygous mutation carriers} \\ \theta_1 \cdot \theta_3 & \text{if homozygous mutation carriers} \end{cases} \quad (8)$$

where θ_1 is the population average CL/*F* for wild-type individuals (e.g. –1818T/T), θ_2 and θ_3 are the fractional change in θ_1 with different mutant genotypes (e.g. –1818T/C or –1818C/C) where possible. Each SNP in UGT1A9 was tested individually.

Model evaluation

The validity of the population PK model was assessed by graphical analysis (goodness-of-fit plots). Basic goodness-of-fit plots including individual predictions (IPRED) *vs.* observed concentrations (DV), as well as weighted residuals (WRES) *vs.* predictions, and the distribution of the WRES with time after dose, were used for diagnostic purposes.

The cross-validation method was applied to assess the contribution of data from individuals on the modelling results and to confirm the robustness of the final model. The full dataset was randomly divided into seven groups, each containing six subjects. Seven different subsets of six groups were then constituted. Each subset of data was analysed by NONMEM using the final model. The parameter estimates for each of the seven runs were obtained and were compared with those resulting from the whole dataset. To test the predictive performance of the final model, the NONMEM estimates from each of the seven subsets were used to predict the plasma profiles in the remaining one group patients' data (six subjects), using the *post hoc* option. Then, the prediction error (PE) and root mean square prediction error (RMSE) in the difference between IPRED and DV were calculated and summarized using descriptive statistics [34]. The PE was used as a measure of model bias and RMSE was used as a measure of model precision [34].

The PK model was also evaluated using a predictive check [35]. Two hundred and fifty datasets of MPA and MPAG were simulated from the final model parameter estimates using the original dataset as a template to define an empirical covariate distribution. Median and 90th percentile of the simulated concentrations were calculated at each time point and were plotted with the observed data. The distribution of the observations was visually compared with the simulated distribution. In addition, AUCs were calculated by noncompartmental analysis using WinNonlin (Version 4.1; Pharsight Corp., Mountain View, CA, USA) for both the simulated and observed data. Student's *t*-test and a Kolmogorov–Smirnov (KS) test were used to determine if the simulated and the true distributions of AUC estimates could have arisen from the same distribution. The AUC statistics was selected for evaluation, because this parameter was the most relevant index of drug exposure and was expected to vary based on concentration and other relevant covariates.

Results

Forty-two healthy male subjects were enrolled. Their demographic characteristics are presented in Table 1. The frequency distribution of the UGT1A9 polymorphisms is given in Table 2. –275T/A and –2152C/T polymorphisms were not found in this study cohort and only one individual was identified as a carrier of a functional UGT1A9*3 allele.

Pharmacokinetics

Mean DV and IPRED profiles of MPA and MPAG are shown in Figure 1. MPA reached its first peak rapidly around 0.5 h postdose, followed by an initial quick decline in all subjects. Subsequently, 20 of 22 individuals in study 2 showed an obvious second arise around 4–6 h postdose. Due to lack of 5 h postdose sampling (1 h after lunch), only three of 20 individuals showed notable peaks around 6 h postdose in study 1. All subjects displayed multiple peaks around 10–12 h postdose. The timing corresponded approximately to mealtime and was consistent with food intake stimulation GB emptying. The pattern of MPAG profile was similar to that of MPA, but was dampened and delayed compared with the latter. The first peak plasma MPAG concentrations occurred around 1.5 h postdose, 1 h after that of MPA. All subjects displayed a second peak around 10–12 h postdose, while only one subject displayed three peaks at around 1.5, 6 and 12 h postdose.

Model building

A total of 590 MPA and 589 MPAG concentration–time measurements were employed in the model establishment. Visual inspection of the curves revealed that MPA

Table 1

Characteristics of subjects studied ($n = 42$)

Characteristics	Mean ± SD	Median (range)
Weight (kg)	67.0 ± 7.63	65.5 (56.5–89.0)
Height (m)	1.73 ± 0.0638	1.73 (1.57–1.86)
Age (years)	21.6 ± 1.68	21 (19–26)
Serum albumin (g l^{-1})	44.9 ± 1.98	45 (40.5–50.0)
Haemoglobin (g l^{-1})	149 ± 8.69	149 (133–172)
Serum creatinine (μmol l^{-1})	73.8 ± 9.53	75.5 (49.5–94.0)
Creatinine clearance (ml min^{-1})	135 ± 23.2	133 (98–194)

Table 2

Frequency distribution of UGT1A9 polymorphisms with Hardy–Weinberg (HW) equilibrium χ^2 and HW *P*-values in 42 healthy volunteers

Position	SNP	*n*	Identified frequency, %	Allele	Allelic frequency, %	HW χ^2	HW *P*-value
–2208	C/C	42/42	100	C	100	NA	1
	C/T	0/42	0	T	0		
	T/T	0/42	0				
–2152	C/C	42/42	100	C	100	NA	1
	C/T	0/42	0	T	0		
	T/T	0/42	0				
–2141	C/C	42/42	100	C	100	NA	1
	C/T	0/42	0	T	0		
	T/T	0/42	0				
–1887	T/T	35/42	83.3	T	90.5	1.23	0.27
	T/G	6/42	14.3	G	9.5		
	G/G	1/42	2.4				
–1818	T/T	10/42	23.8	T	47.6	0.087	0.77
	T/C	20/42	47.6	C	52.4		
	C/C	12/42	28.6				
–665	C/C	42/42	100	C	100	NA	1
	C/T	0/42	0	T	0		
	T/T	0/42	0				
–440	T/T	0/0	0	T	2.4	0.025	0.87
	T/C	2/42	4.8	C	97.6		
	C/C	40/42	95.2				
–331	C/C	0/42	0	C	2.4	0.025	0.87
	C/T	2/42	4.8	T	97.6		
	T/T	40/42	95.2				
–275	T/T	42/42	100	T	100	NA	1
	T/A	0/42	0	A	0		
	A/A	0/42	0				
–109 to –98 T(n)	9/9	20/42	47.6	9	50	34.4	<0.001
	9/10	2/42	4.8	10	50		
	10/10	20/42	47.6				
–87	G/G	41/42	97.6	G	98.8	0.0061	0.94
	G/A	1/42	2.4	A	1.2		
	A/A	0/42	0				
+98	T/T	41/42	97.6	T	98.8	0.0061	0.94
	T/C	1/42	2.4	C	1.2		
	C/C	0/42	0				

NA, not available.

was best described by a two-compartment model, whereas MPAG could be described by a one-compartment model. In addition, a model with first-order absorption of MPA fitted better than one with zero order absorption with a 140 point lower OFV, and introduction of lag time further decreased the OFVs by 107. A schematic diagram of the proposed model is shown in Figure 2. In order to describe the profile of MPA and MPAG, two circumstances were considered, i.e. absence and presence of GB emptying. Assuming all the kinetic processes were first order, the differential equations for the change in the amount of substance with time in the absence of GB emptying are shown below:

$$\frac{dX_1}{dt} = -k_{12} \cdot X_1 \tag{9}$$

$$\frac{dX_2}{dt} = k_{12} \cdot X_1 - (k_{23} + k_{20}^*) \cdot X_2 + k_{32} \cdot X_3 \tag{10}$$

$$\frac{dX_3}{dt} = k_{23} \cdot X_2 - k_{32} \cdot X_3 \tag{11}$$

$$\frac{dX_4}{dt} = f_m \cdot k_{20}^* \cdot X_2 - (k_{40} + k_{45}) \cdot X_4 \tag{12}$$

$$\frac{dX_5}{dt} = k_{45} \cdot X_4 \tag{13}$$

$$k_{20}^* = k_{20} + k_{24} \tag{14}$$

$$k_{24} = f_m \cdot k_{20}^* \tag{15}$$

where X_n represent the drug amount in the *n*th compartment. The compartments are defined as follows: 1 the GI compartment; 2 the central compartment of MPA; 3 the peripheral compartment of MPA; 4 the central compart-

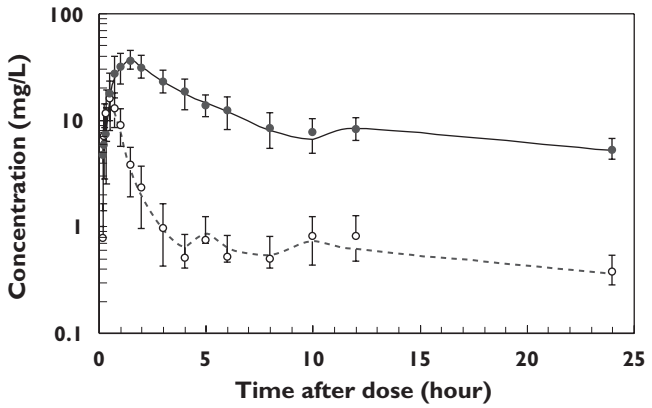

Figure 1

Mean observed and individual Bayesian predicted plasma concentration–time curves with standard deviation (SD) for mycophenolic acid (MPA) and 7-O-glucuronide (MPAG) after administration of a single oral dose of 500 mg mycophenolate mofetil ($n = 42$). Filled circle and open circle represent observed MPAG and MPA concentration, respectively; solid lines and dots denote the predicted MPAG and MPA, respectively; the upward and downward error bars represent SD of observed and predicted concentration, respectively

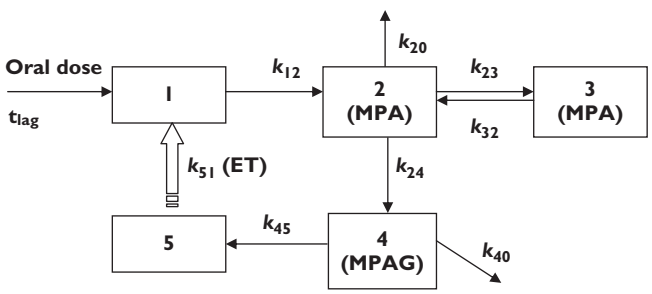

Figure 2

The enterohepatic circulation model used for mycophenolic acid (MPA) and mycophenolic acid 7-O-glucuronide (MPAG) analysis. Compartment: 1, gastrointestinal tract; 2, central compartment of MPA; 3, peripheral compartment of MPA; 4, central compartment of MPAG; 5, gall bladder. k_{ij}, rate constant among compartments; t_{lag}, lag time in absorption phase; ET, gallbladder empting time; $k_{20}^{*} = k_{20} + k_{24}$

ment of MPAG; 5 the GB compartment; k_{ij} are the rate constants among the compartments.

During the GB emptying window, assuming all MPAG secreted from GB to intestine were completely converted to MPA and was followed by reabsorption into the system, the equations representing the MPA change in compartment 1 and 5 are defined by Equations 16 and 17.

$$\frac{dX_1}{dt} = -k_{12} \cdot X_1 + k_{51} \cdot X_5 \tag{16}$$

$$\frac{dX_5}{dt} = k_{45} \cdot X_4 - k_{51} \cdot X_5 \tag{17}$$

Two EHCs in the first 24 h after administration were modelled in the present study. Model structural identifiability analysis (see Appendix), which refers to uniquely estimating a model's parameters, indicated that several assumptions needed to be made prior to model development: (i) the conversion ratio from MPA to MPAG (f_m) was fixed at 100%; (ii) the rate constants associated with each compartment were not affected by the recycling; and (iii) the two EHC processes were exactly the same.

Since insufficient data were collected around the EHC process, several parameters needed to be fixed based on prior information to make the model numerically identifiable, which refers to accurate and precise estimation of a structurally identifiable model's parameters given real, observed data [29, 36]: (i) it is known that food stimulates bile secretion and that GB emptying is postulated to be at mealtime, i.e. at 4 and 10 h postdose in the first study and 4 and 9.5 h postdose in the second study; (ii) release of bile was assumed to occur as a bolus (assuming emptying duration was 0.01 h) at the time of expulsion from the GB [36].

The following PK parameters were estimated: absorption rate constant (k_{12}), time lag between intake and start absorption (t_{lag}), apparent volume of distribution (V_2/F for MPA central compartment, V_3/F for MPA peripheral compartment and V_4/F for MPAG compartment), apparent clearance of MPA (CL_{MPA}/F, $CL_{MPA}/F = k_{20}^{*} \cdot V_2/F$), apparent intercompartmental clearance of MPA (Q/F), apparent renal clearance of MPAG (CL_{MPAG}/F, $CL_{MPAG}/F = k_{40} \cdot V_4/F$), the rate constant between GB and GI compartment (k_{51}), and the percentage of MPA recycled into the body (EHCP, Equation 18).

$$EHCP = \frac{k_{45}}{k_{40} + k_{45}} \times 100\% \tag{18}$$

Inter-individual variability terms were tested initially on all the PK parameters. The interindividual variability of k_{51} was very small and could be eliminated without significantly altering the parameter values or the OFV. Therefore, it was excluded for the rest of the model-building process.

GAM analysis showed that body weight had an influence on V_2/F, V_3/F, Q/F and CL_{MPA}/F, and that creatinine clearance had an influence on CL_{MPAG}/F. Polymorphisms of UGT1A9 did not show any influence on CL_{MPA}/F. After a stepwise screening procedure, only body weight on Q/F, V_3/F and CL_{MPA}/F was identified as an important covariate, and the slope linear model without intercept was selected according to the OFV value. Inclusion of body weight as covariate decreased the OFV by 20.1, 11.8 and 10.2, respectively, and reduced interindividual variability of Q/F, V_3/F and CL_{MPA}/F by 26.5%, 34.8% and 15.9%, respectively.

Inspection of the posterior η distributions indicated there was a correlation between $\eta(CL_{MPAG}/F)$ and $\eta(Q/F)$. Inclusion of this correlation gave significant reductions of 11.2 in the OFV and was adopted in the final model.

Table 3

Pharmacokinetic parameter estimates in the full dataset and in seven different subsets using the final model

Parameter	Full dataset			Subset						
Pharmacokinetic parameters	Mean	SE%	95% CI	1	2	3	4	5	6	7
t_{lag} (h)	0.0956	15.8	0.0660, 0.125	0.115	0.0882	0.097	0.0916	0.0905	0.0904	0.0981
k_{12} (h^{-1})	3.53	12.4	2.67, 4.39	3.70	3.16	3.68	3.19	3.57	3.55	3.79
Q/F (l h^{-1})	16.1	5.10	14.5, 17.7	16.1	16.2	15.9	16.6	16.3	16.3	15.8
CL_{MPA}/F (l h^{-1})	10.2	5.70	9.06, 11.3	10.3	10.1	9.97	9.87	10.1	10.4	10.5
CL_{MPAG}/F (l h^{-1})	1.38	6.90	1.19, 1.57	1.39	1.29	1.36	1.44	1.36	1.41	1.37
V_2/F (l)	12.5	8.30	10.5, 14.5	12.0	12.1	12.8	12.0	12.6	12.4	12.8
V_3/F (l)	213	9.10	175, 251	206	237	213	216	218	201	212
V_4/F (l)	4.40	6.40	3.85, 4.95	4.40	4.30	4.40	4.41	4.38	4.40	4.41
EHCP	29.1	10.4	23.2, 35.0	28.1	30.8	29.3	26.5	29.1	27.8	32.0
k_{51} (h^{-1})	67.5	12.7	50.7, 84.3	68.0	73.4	62.0	79.7	71.4	62.0	64.8
Interindividual variability (%)										
t_{lag}	57.3	44.5	7.32, 107	39.4	64.6	55.4	63.3	61.6	63.3	53.9
k_{12}	60.3	31.9	22.6, 98.6	73.1	60.6	58.2	57.4	61.7	59.5	55.6
Q/F	13.7	48.9	0.570, 32.1	15.7	17.0	12.0	7.70	14.0	15.3	14.1
CL_{MPA}/F	18.9	35.6	5.71, 26.8	16.1	18.6	19.8	16.8	19.4	20.3	19.6
V_2/F	34.5	48.7	1.57, 67.4	16.5	37.8	32.2	40.0	36.7	36.7	31.5
V_3/F	22.7	39.2	5.26, 40.1	22.0	24.9	22.6	20.6	23.7	21.6	22.5
V_4/F	23.1	37.3	6.21, 40.0	25.0	21.8	24.9	22.2	22.9	23.5	21.6
EHCP	29.0	49.3	0.979, 57.1	32.1	26.9	28.7	27.1	30.5	31.5	24.8
θ	1.33	27.2	0.621, 2.04	1.21	0.985	1.48	1.89	1.30	1.29	1.42
Residual variability (%)										
ε for MPA	45.3	9.30	37.0, 53.5	43.7	44.5	45.4	44.6	45.5	46.4	46.3
ε for MPAG	20.8	16.3	14.1, 27.4	20.0	21.2	20.7	21.4	21.2	21.2	19.5

$\eta_{CLMPAG/F} = \theta \cdot \eta_Q$; SE%, relative standard error percentage; 95% CI, 95% confidence interval.

Moreover, an exponential model provided the best results for residual variability of both MPA and MPAG.

In the final step of model building, the parameters were estimated by several advanced approaches. FOCE and FOCE-I without data log transformation both converged successfully and provided similar structural parameter estimates except K_a and T_{lag}. Since in most cases FOCE-I provide more accurate estimates of model parameters than FOCE, it was the estimation method of choice for the final model [29, 37, 38]. Moreover, the covariate effects and the correlation between $\eta(CL_{MPAG}/F)$ and $\eta(Q/F)$ were confirmed using FOCE-I. The PK parameter estimates of the final model are listed in Table 3. The typical population CL/F values with relative standard error for MPA and MPAG were 10.2 l h^{-1} (5.7%) and 1.38 l h^{-1} (6.9%), respectively. The percentage of MPA recycled into the central compartment was estimated to be 29.1% of the total amount absorbed.

The influence of duration of GB emptying was investigated. The emptying time window was tested from 0.01 to 0.5 h. Only k_{51} changed accordingly and other structural parameter estimates changed by no more than 4%. The model was also tested to estimate the GB emptying time by fixing k_{51} to a large value. This led to failure in model convergence due to numerical difficulties. Incorporation of interindividual variability for GB emptying time and its duration did not achieve the model convergence either. These unsuccessful convergences could be indicative of over-parameterization and may be attributed to lack of information around mealtime.

Model evaluation

The basic goodness-of-fit plots of the final model for MPA and MPAG are presented in Figures 3 and 4, respectively. No obvious systematic deviation can be seen. However, slight over- and underestimation of MPA around the first and second EHC occurring, respectively, can be observed in Figure 3c, indicating that two EHC processes may not be the same. Since these divergences are within acceptable limits (>96% of both MPA and MPAG values are within ± 2 WRES), we conclude that the final model describes the data reasonably.

The cross-validation results are presented in Table 3. The PK parameters for the seven subsets are within 95% confidence interval (CI) of the estimates obtained from the entire database. The comparison between the IPRED and DV for each subset showed mean PE (95% CI) of 0.149 (–0.124, 0.422) and 0.153 mg l^{-1} (–0.570, 0.263) as well as mean RMSE (95% CI) of 2.84 (2.57, 3.12) and 3.35 mg l^{-1} (2.73, 3.97) for the MPA and MPAG, respectively.

The results of the visual predictive check evaluation are presented in Figure 5. Most of the observations are well contained within the prediction intervals, except that slight overestimation of 90% percentiles of MPAG could be observed, which may indicate imprecise parameter estimates of MPAG variability. The results from the *t*-test

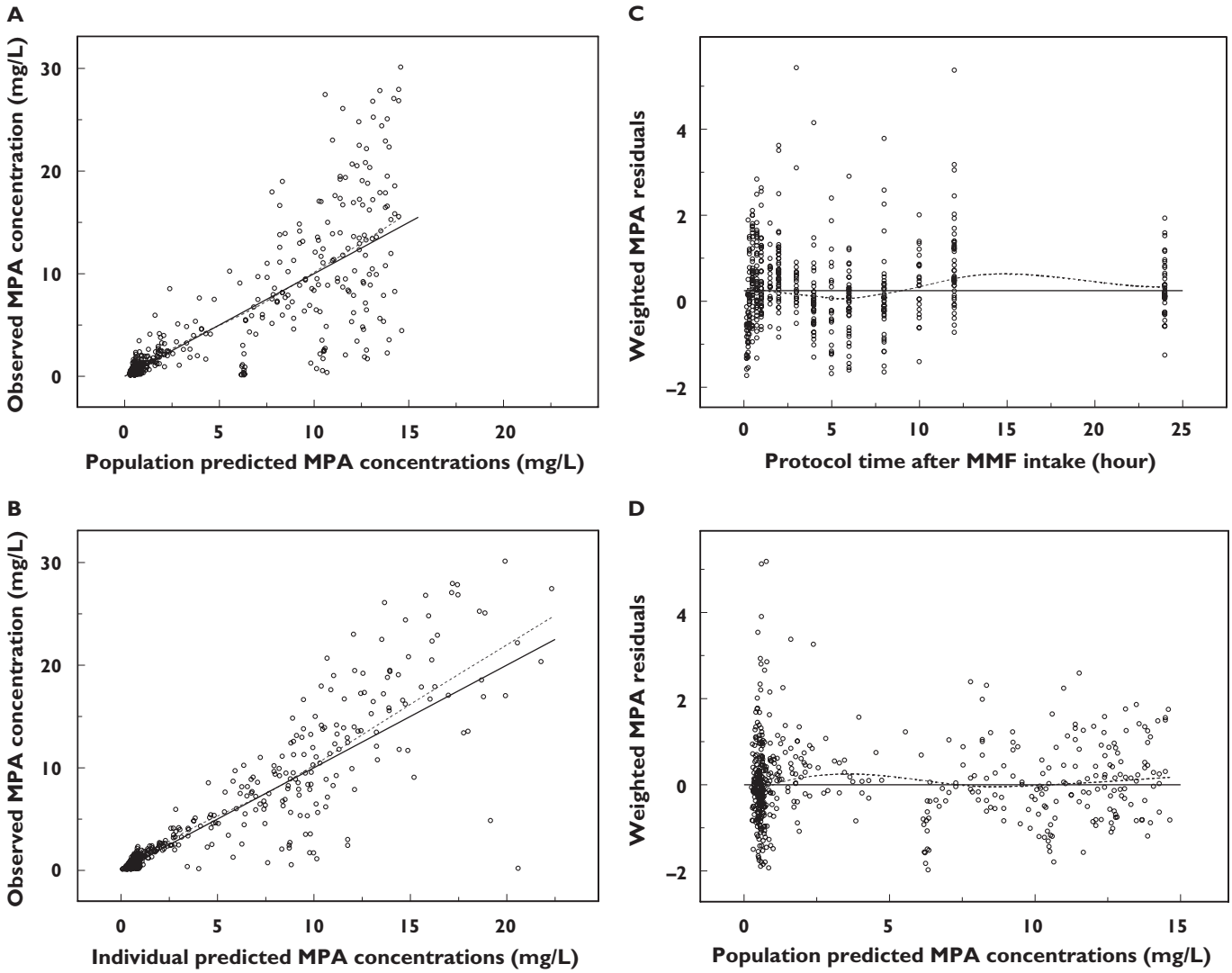

Figure 3

Model evaluation plots. (a) Population predicted mycophenolic acid (MPA) concentration *vs.* observed MPA concentration. (b) Individual Bayesian predicted MPA concentration *vs.* observed MPA concentration. (c) Protocol sample time *vs.* weighted residuals and (d) population predicted MPA concentrations *vs.* time. The solid lines in (a) and (b) represent the line of identity and those in (c) and (d) represent the line y = 0. The dotted lines in each panel represent loess smooth of the data

($P > 0.80$ for both MPA and MPAG) and KS test ($P > 0.64$ for both MPA and MPAG) suggested that the AUC values from simulated datasets were similar both for the mean values and for the distribution of observed AUC. Hence, all model evaluations indicated that the model was adequate in characterizing the PK profile of MPA and MPAG.

Discussion

To our knowledge, this is the first report on the population PK of MPA and MPAG in the Chinese population. Based on physiological considerations, we proposed a new PK model to describe the EHC process by incorporating both MPA and MPAG simultaneously with intensive sampling data. In addition, the model structural identifiability was checked and several assumptions were made prior to PK modelling so that observed data could uniquely specify the basic kinetic parameters. This is an important test, since insufficiencies or inappropriateness in the experimental input–output design may lead to bias or failure in model building and parameter estimation, especially in complicated PK settings [10, 11].

The multiple peaks arising from EHC are well characterized in the current model. The evaluation tests, including graphical analysis, cross-validation and the predictive check show that the final proposed model could describe the data adequately. However, the residual error in MPA

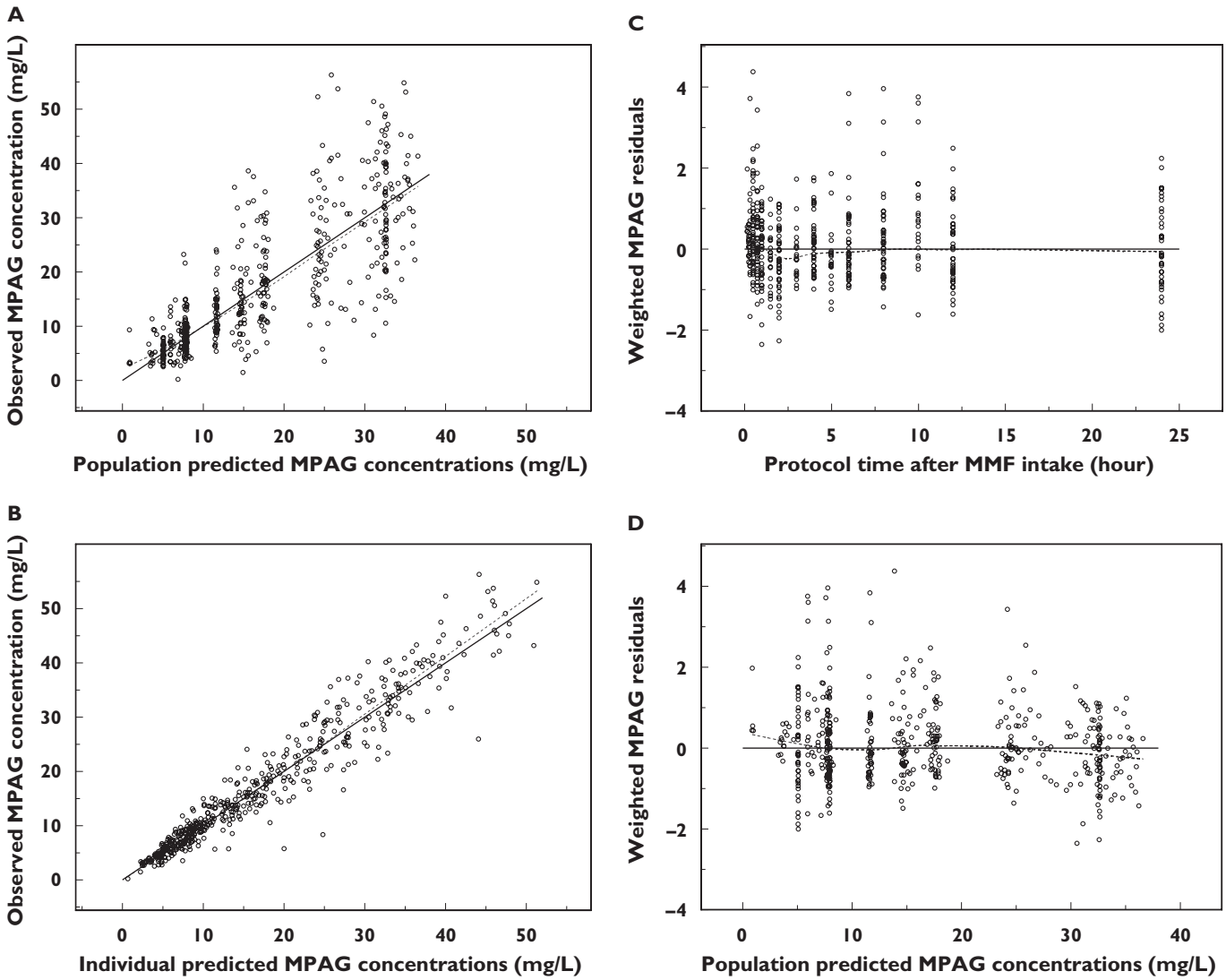

Figure 4

Model evaluation plots. (a) Population predicted mycophenolic acid 7-O-glucuronide (MPAG) concentration *vs.* observed MPAG predicted concentration. (b) Individual Bayesian predicted MPAG concentration *vs.* observed MPAG concentration. (c) Protocol sample time *vs.* weighted residuals and (d) population predicted MPAG predicted concentrations *vs.* time. The solid lines in (a) and (b) represent the line of identity and those in (c) and (d) represent the line y = 0. The dotted lines in each panel represent loess smooth of the data

modelling was relatively high, which may be attributed to some of the assumptions made to retain model identifiability.

In our model it was assumed that all MMF were converted to MPA, following complete metabolism to MPAG, with no other metabolites or elimination processes being present. This is known to be an inaccurate representation of the true fate of MPA [14]. According to the model structural identifiability analysis, determination of f_m and F by conducting additional urine and intravenous PK studies in the same study cohort could help to improve the model estimates.

In addition, GB emptying was postulated to be at mealtime and each process was assumed to be the same. The rate constants associated with each compartment were also assumed not to be affected by the recycling. However, this may not be true under normal conditions. GB emptying may occur on the sight, smell or ingestion of food, and the extent of biliary emptying may depend on the quantity of fat in the meal [12]. More sampling around mealtime could provide more accurate assessment of the timing and magnitude of the EHC process.

Furthermore, high interindividual variation in k_{12} and t_{lag} could be seen. This is not unexpected, since the input process of MPA is considerably more complicated than a single first-order process, which includes absorption of MMF and conversion to MPA. The high variation in these parameters may indicate some degree of misspecification

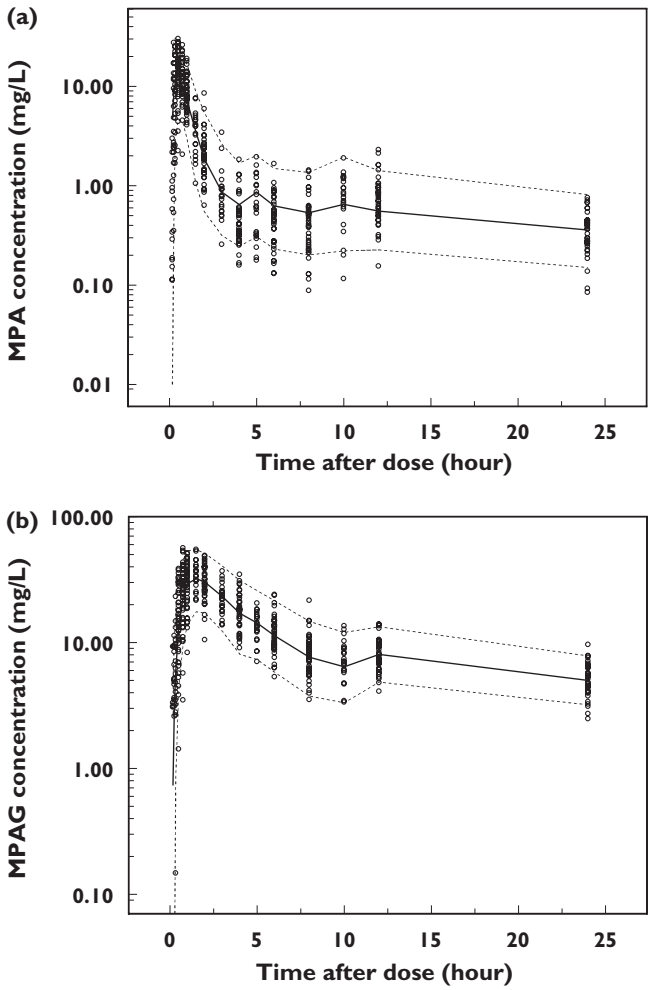

Figure 5

A visual assessment of the posterior predictive performance of the pharmacokinetic model in terms of its ability to predict the observed plasma. (a) Mycophenolic acid (MPA) and (b) mycophenolic acid 7-O-glucuronide (MPAG) concentration–time profile. The lines represent the 5th, 50th and 95th percentiles of concentration distribution in each panel

in the input process and may also play a significant role in the large residual error of MPA.

The typical values of the MPA and MPAG CL/*F* in healthy Chinese were about 0.156 l h^{-1} kg^{-1} and 0.0211 l h^{-1} kg^{-1}, respectively. Since no sex difference was observed in the previous MPA PK study [39], the results from male Chinese could be compared to the patients in stable post-transplant periods. Cremer *et al.* [6] recently conducted a population PK analysis in White renal transplant patients who had normal renal function 3 months after transplantation. CL/*F* of MPA and MPAG were reported to be 0.158 l h^{-1} kg^{-1} and 0.0144 l h^{-1} kg^{-1}, respectively, in patients on tacrolimus, which does not influence the EHC of MPA [40–42]. The value of MPA CL/F is very close to that of the present study, indicating that there may be no pronounced ethnicity difference in MPA CL/*F*. This result is also consistent with previous observations in Chinese [43–46] and Korean [47] renal transplant patients. In terms of MPAG CL/*F*, the typical value of healthy Chinese was 46% higher than that of stable White renal transplant recipients. Due to the lack of standard deviation values in the previous study, the CL/*F* of MPAG may not be compared directly between these two studies. However, the trend of higher MPAG CL/*F* in the Chinese population was obvious, supporting the previous findings that MPAG exposure was twofold higher in White renal transplant patients than in Chinese patients during the first month post transplantation [43, 46]. The reason is unclear, and this may need to be clarified in future investigations.

For drugs that are excreted extensively into the bile, insight into the magnitude of EHC is of crucial importance, as it will significantly affect PK parameters such as plasma half-life, AUC and estimates of bioavailability. The mean MPA circulation ratio is estimated to be 29.1% of the total amount absorbed, which is also consistent with the values in previous reports of 25% [6] or approximately 40% (range 10–60%) [4].

MPA exposure is characterized by large intra- and inter-individual variability that changes over time. Body weight [14, 48], renal graft function [48–53], serum albumin binding [53, 54], haemoglobin concentration [48, 53] and drug interactions with calcineurin inhibitors and mammalian target of rapamycin inhibitors [6, 40, 41, 55–58] are identified as determinants. Due to the homogeneity of the current study cohort, only total body weight was identified as having a significant influence on CL_{MPA}/F, Q/F and V_3/F, which further confirms the observations from Whites.

Differences in the genotype and phenotype of drug-metabolizing enzymes involved in MPA biotransformation may be associated with interindividual variability in response to MMF therapy. Several studies have investigated the polymorphisms of UGT on the PK of MPA [22, 23, 59]. However, most [22, 23] were conducted in renal transplant patients and the results could be complicated by comedication and disease status. As little information has been obtained from Chinese so far, we have genotyped the SNPs of UGT1A9 and investigated the effect of polymorphism in healthy subjects. Using the proposed EHC model, it was possible to assess all factors influencing the PK compared with the conventional noncompartmental method, and the analysis results were less biased by the effects of EHC. Because the microsomal systems may not reflect *in vivo* activity [60], not only the effect of –2152/–275 and UGT1A9*3 polymorphism, which was proved to be the determinant of MPA disposition [22, 23, 59], but also that of other SNPs reported previously [17] were investigated.

In this study cohort, we did not find –2152/–275 polymorphism, which is consistent with the results from other studies conducted in the Japanese [23, 24]. Only one individual was a carrier of a functional UGT1A9*3 allele and hence it is not unexpected that no effects on MPA/MPAG PK characteristics were observed. Moreover, we found no relationship between other polymorphisms in UGT1A9

promoter and MPA/MPAG disposition either. Since MPAG is also formed by UGT1A7, 1A8, 2B7 and 1A10 [16–20,61] and its excretion into bile and urine involves multidrug resistance protein 2 (MRP-2)-mediated transportation [12, 41, 42, 62], it is of interest to perform further investigation with complete and detailed genetic profiling of UGT and MRP2.

In addition, our study has further demonstrated that occurrence of the MPA EHC process corresponded to the food taken. Lack of sampling around mealtime could lead to failure in detection of multiple peaks in the plasma concentration *vs.* time profiles. It also implies that when establishing the limited sampling strategy for MPA monitoring, the influence of mealtime may not be neglected. However, little attention has been paid to this issue in previous studies, which may partly explain the large discrepancies in the reported limited sampling strategies [13, 15, 63].

In conclusion, a population PK model for MPA and its main glucuronide metabolite MPAG, that included additional input due to EHC, was developed. This model was selected based on physiological considerations and statistical and graphical criteria such as model structural identifiability analysis and visual predictive check. In addition, the population PK of MPA and MPAG with the effect of UGT 1A9 polymorphism in healthy Chinese was characterized using the proposed model. Our study provides a valuable approach to planning future pharmacokinetic–pharmacodynamic studies and for designing proper dosage regimens of MPA in clinical settings.

Appendix

Model identifiability analysis [11]

A linear system can be described by the general form as:

$$\frac{dx}{dt} = Ax + Bu \tag{1}$$

$$y = Cx \tag{2}$$

where A is the $(n \times n)$ system matrix, B is the input matrix, and C is the output matrix. As a technical point, it is assumed that two different sets of parameter values cannot give rise to the same matrices A, B, and C.

$$A = \begin{pmatrix} a_{11} & a_{12} & . & . & a_{1n} \\ a_{21} & . & . & . & . \\ . & . & . & . & . \\ . & . & . & . & . \\ a_{n1} & . & . & . & a_{nn} \end{pmatrix} \tag{3}$$

$$B = \begin{pmatrix} b_{11} & b_{12} & . & . & b_{1i} \\ b_{21} & . & . & . & . \\ . & . & . & . & . \\ . & . & . & . & . \\ b_{n1} & . & . & . & b_{ni} \end{pmatrix} \tag{4}$$

$$C = \begin{pmatrix} c_{11} & c_{12} & . & . & c_{1n} \\ c_{21} & . & . & . & . \\ . & . & . & . & . \\ . & . & . & . & . \\ c_{i1} & . & . & . & c_{in} \end{pmatrix} \tag{5}$$

Provided a system is controllable and observable, it is then possible to proceed with the identifiability analysis using the similarity transformation approach. This utilizes the fact that, for another model, characterized by $(\bar{A}, \bar{B}, \bar{C})$, to have identical input–output behaviour, it is necessary and sufficient that there exists a nonsingular matrix T such that

$$T \cdot \bar{B} = B \tag{6}$$

$$\bar{C} = C \cdot T \tag{7}$$

$$T \cdot \bar{A} = A \cdot T \tag{8}$$

The model characterized by $(\bar{A}, \bar{B}, \bar{C})$ is assumed to have the same structure as the original, but possibly different parameter values. Hence, if any entry in A (respectively, B or C) is zero then the corresponding entry in the matrix (respectively,) is also zero. If these three equations taken together imply that T is the $n \times n$ identity matrix, then the model is globally identifiable.

To test the structural identifiability of the proposed model described in Figure 2, two circumstances were considered to describe the profile of MPA and MPAG, i.e. absence and presence of gallbladder emptying.

In the absence of gallbladder emptying, the system matrix A, input matrix B and output matrix C for the proposed model were expressed as (Equations 9–11)

$$A = \begin{pmatrix} -k_{12} & 0 & 0 & 0 & 0 \\ k_{12} & -k_{20}^{*} - k_{23} & k_{32} & 0 & 0 \\ 0 & k_{23} & -k_{32} & 0 & 0 \\ 0 & f_m k_{20}^{*} & 0 & -k_{40} - k_{45} & 0 \\ 0 & 0 & 0 & k_{45} & 0 \end{pmatrix} \tag{9}$$

$$B = \begin{pmatrix} 1 \\ 0 \\ 0 \\ 0 \\ 0 \end{pmatrix} \tag{10}$$

$$C = \begin{pmatrix} 0 & \frac{1}{V_2} & 0 & 0 & 0 \\ 0 & 0 & 0 & \frac{1}{V_4} & 0 \end{pmatrix} \tag{11}$$

Let P, given by

$$P = (f_m \quad k_{12} \quad k_{23} \quad k_{32} \quad k_{20}^* \quad k_{40} \quad k_{45} \quad F_1 \quad V_2 \quad V_4)^T \quad (12)$$

denote the vector of unknown positive parameters, in which $k_{20}^* = k_{20} + k_{24}$. By substituting A, B, C into equations 6–8, and solving this set of equations, the solution is obtained. Thus k_{12}, k_{23}, k_{32}, k_{20}^*, $k_{40} + k_{45}$, $f_m \cdot k_{20}^* / V_4$, are uniquely identifiable, while k_{20}, k_{24}, k_{40}, k_{45}, V_2 and V_4 are not identifiable. If absolute bioavailability and conversion ratio of MPA to MPAG were known *a priori*, k_{24}, k_{20}, V_2 and V_4 would be globally identifiable.

During the gallbladder emptying window, the system matrix A is expressed differently as shown below (Equation 13), whereas the other matrixes B, C remain the same.

$$A = \begin{pmatrix} -k_{12} & 0 & 0 & 0 & k_{51} \\ k_{12} & -k_{20}^* - k_{23} & k_{32} & 0 & 0 \\ 0 & k_{23} & -k_{32} & 0 & 0 \\ 0 & f_m k_{20}^* & 0 & -k_{40} - k_{45} & 0 \\ 0 & 0 & 0 & k_{45} & -k_{51} \end{pmatrix} \quad (13)$$

The test of structural identifiability under this condition is performed using a similar approach to that above. Summarizing the results, only k_{51} and k_{45} are uniquely identifiable.

Assuming the rate constants associated with each compartment are not affected by the recycling, i.e. k_{12}, k_{23}, k_{32}, k_{20}^*, $k_{40} + k_{45}$, $f_m \cdot k_{20}^* / V_4$, k_{24}, k_{20}, V_2 and V_4 were unchanged and identifiable, all parameters will be globally identifiable.

This work was partly supported by Shanghai Natural Science Fund (03ZR14010). The authors thank Professor Keith Godrey (School of Engineering, University of Warwick, UK) for his suggestions on the model structural identifiability analysis. The authors are also grateful to two anonymous reviewers for their critical reviews and valuable comments.

REFERENCES

1 The Tricontinental Mycophenolate Mofetil Renal Transplantation Study Group. A blinded, randomized clinical trial of mycophenolate mofetil for the prevention of acute rejection in cadaveric renal transplantation. Transplantation 1996; 61: 1029–37.

2 European Mycophenolate Mofetil Cooperative Study Group. Placebo-controlled study of mycophenolate mofetil combined with cyclosporin and corticosteroids for prevention of acute rejection. Lancet 1995; 345: 1321–5.

3 Sollinger HW. Mycophenolate mofetil for the prevention of acute rejection in primary cadaveric renal allograft recipients. U.S. Renal Transplant Mycophenolate Mofetil Study Group. Transplantation 1995; 60: 225–32.

4 Bullingham RE, Nicholls A, Hale M. Pharmacokinetics of mycophenolate mofetil (RS61443): a short review. Transplant Proc 1996; 28: 925–9.

5 Funaki T. Enterohepatic circulation model for population pharmacokinetic analysis. J Pharm Pharmacol 1999; 51: 1143–8.

6 Cremers S, Schoemaker R, Scholten E, den Hartigh J, Konig-Quartel J, van Kan E, Paul L, de Fijter J. Characterizing the role of enterohepatic recycling in the interactions between mycophenolate mofetil and calcineurin inhibitors in renal transplant patients by pharmacokinetic modelling. Br J Clin Pharmacol 2005; 60: 249–56.

7 Premaud A, Debord J, Rousseau A, Le Meur Y, Toupance O, Lebranchu Y, Hoizey G, Le Guellec C, Marquet P. A double absorption-phase model adequately describes mycophenolic acid plasma profiles in *de novo* renal transplant recipients given oral mycophenolate mofetil. Clin Pharmacokinet 2005; 44: 837–47.

8 Jiao Z, Shen J, Zhong LJ, Yu YQ, Zhong MK. Pharmacokinetic model for the enterohepatic circulation of mycophenolic acid. Acta Pharmceutica Sinica 2006; 41: 272–6.

9 Jacquez JA. Parameter identifiability is required in pooled data methods. J Pharmacokinet Biopharm 1996; 24: 301–5.

10 Bellman R, Astrom KJ. On structural identifiability. Math Biosic 1970; 7: 329–39.

11 Evans ND, Godfrey KR, Chapman MJ, Chappell MJ, Aarons L, Duffull SB. An identifiability analysis of a parent-metabolite pharmacokinetic model for ivabradine. J Pharmacokinet Pharmacodyn 2001; 28: 93–105.

12 Roberts MS, Magnusson BM, Burczynski FJ, Weiss M. Enterohepatic circulation: physiological, pharmacokinetic and clinical implications. Clin Pharmacokinet 2002; 41: 751–90.

13 Staatz CE, Tett SE. Clinical pharmacokinetics and pharmacodynamics of mycophenolate in solid organ transplant recipients. Clin Pharmacokinet 2007; 46: 13–58.

14 Bullingham RE, Nicholls AJ, Kamm BR. Clinical pharmacokinetics of mycophenolate mofetil. Clin Pharmacokinet 1998; 34: 429–55.

15 van Gelder T, Meur YL, Shaw LM, Oellerich M, DeNofrio D, Holt C, Holt DW, Kaplan B, Kuypers D, Meiser B, Toenshoff B, Mamelok RD. Therapeutic drug monitoring of mycophenolate mofetil in transplantation. Ther Drug Monit 2006; 28: 145–54.

16 Bernard O, Guillemette C. The main role of UGT1A9 in the hepatic metabolism of mycophenolic acid and the effects of naturally occurring variants. Drug Metab Dispos 2004; 32: 775–8.

17 Girard H, Court MH, Bernard O, Fortier LC, Villeneuve L, Hao Q, Greenblatt DJ, von Moltke LL, Perussed L, Guillemette C. Identification of common polymorphisms in the promoter of the UGT1A9 gene: evidence that UGT1A9 protein and activity levels are strongly genetically controlled in the liver. Pharmacogenetics 2004; 14: 501–15.

18 Picard N, Ratanasavanh D, Premaud A, Le Meur Y, Marquet P. Identification of the UDP-glucuronosyltransferase isoforms

involved in mycophenolic acid phase II metabolism. Drug Metab Dispos 2005; 33: 139–46.

19 Bernard O, Tojcic J, Journault K, Perusse L, Guillemette C. Influence of nonsynonymous polymorphisms of UGT1A8 and UGT2B7 metabolizing enzymes on the formation of phenolic and acyl glucuronides of mycophenolic acid. Drug Metab Dispos 2006; 34: 1539–45.

20 Miles KK, Kessler FK, Smith PC, Ritter JK. Characterization of rat intestinal microsomal UDP-glucuronosyltransferase activity toward mycophenolic acid. Drug Metab Dispos 2006; 34: 1632–9.

21 Yamanaka H, Nakajima M, Katoh M, Hara Y, Tachibana O, Yamashita J, McLeod HL, Yokoi T. A novel polymorphism in the promoter region of human UGT1A9 gene (UGT1A9*22) and its effects on the transcriptional activity. Pharmacogenetics 2004; 14: 329–32.

22 Kuypers DR, Naesens M, Vermeire S, Vanrenterghem Y. The impact of uridine diphosphate-glucuronosyltransferase 1A9 (UGT1A9) gene promoter region single-nucleotide polymorphisms T-275A and C-2152T on early mycophenolic acid dose-interval exposure in *de novo* renal allograft recipients. Clin Pharmacol Ther 2005; 78: 351–61.

23 Kagaya H, Inoue K, Miura M, Satoh S, Saito M, Tada H, Habuchi T, Suzuki T. Influence of UGT1A8 and UGT2B7 genetic polymorphisms on mycophenolic acid pharmacokinetics in Japanese renal transplant recipients. Eur J Clin Pharmacol 2007; 63: 279–88.

24 Saeki M, Saito Y, Jinno H, Sai K, Ozawa S, Kurose K, Kaniwa N, Komamura K, Kotake T, Morishita H, Kamakura S, Kitakaze M, Tomoike H, Shirao K, Tamura T, Yamamoto N, Kunitoh H, Hamaguchi T, Yoshida T, Kubota K, Ohtsu A, Muto M, Minami H, Saijo N, Kamatani N, Sawada JI. Haplotype structures of the UGT1A gene complex in a Japanese population. Pharmacogenomics J 2006; 6: 63–75.

25 Jiao Z, Zhong Y, Shen J, Yu YQ. Simple high-performance liquid chromatographic assay, with post-column derivatization, for simultaneous determination of mycophenolic acid and its glucuronide metabolite in human plasma and urine. Chromatographia 2005; 62: 363–71.

26 Shi YY, He L. SHEsis, a powerful software platform for analyses of linkage disequilibrium, haplotype construction, and genetic association at polymorphism loci. Cell Res 2005; 15: 97–8.

27 Jonsson EN, Karlsson MO. Xpose – an S-PLUS based population pharmacokinetic/pharmacodynamic model building aid for NONMEM. Comput Methods Programs Biomed 1999; 58: 51–64.

28 Boeckmann AJ, Sheiner LB, Beal S. NONMEM Users Guide. San Francisco: University of California: NONMEM project group, 1994–2006.

29 Bonate PL. Nonlinear mixed effects models: practical issues. In: Pharmacokinetic–Pharmacodynamic Modeling and Simulation, 1st edn, ed. Bonate PL. New York: Springer Science and Buisness Media, 2005; 267–72.

30 Hooker AC, Staatz CE, Karlsson MO. Conditional Weighted Residuals (CWRES): a model diagnostic for the FOCE method. Pharm Res 2007; 24: 2187–97.

31 Ette EI, Ludden TM. Population pharmacokinetic modeling: the importance of informative graphics. Pharm Res 1995; 12: 1845–55.

32 Cockcroft DW, Gault MH. Prediction of creatinine clearance from serum creatinine. Nephron 1976; 16: 31–41.

33 Mandema JW, Verotta D, Sheiner LB. Building population pharmacokinetic–pharmacodynamic models. I. Models for covariate effects. J Pharmacokinet Biopharm 1992; 20: 511–28.

34 Sheiner LB, Beal SL. Some suggestions for measuring predictive performance. J Pharmacokinet Biopharm 1981; 9: 503–12.

35 Yano Y, Beal SL, Sheiner LB. Evaluating pharmacokinetic/pharmacodynamic models using the posterior predictive check. J Pharmacokinet Pharmacodyn 2001; 28: 171–92.

36 Gabrielsson J, Weiner D. Enterohepatic recirculation. In: Pharmacokinetic and Pharmacodynamic Data Analysis: Concepts and Applications, 3rd edn, eds Gabrielsson J, Weiner D. Stockholm: Swedish Pharmaceutical Press, 2000; 633–8.

37 Wahlby U, Bouw MR, Jonsson EN, Karlsson MO. Assessment of type I error rates for the statistical sub-model in NONMEM. J Pharmacokinet Pharmacodyn 2002; 29: 251–69.

38 Wahlby U, Jonsson EN, Karlsson MO. Assessment of actual significance levels for covariate effects in NONMEM. J Pharmacokinet Pharmacodyn 2001; 28: 231–52.

39 Pescovitz MD, Guasch A, Gaston R, Rajagopalan P, Tomlanovich S, Weinstein S, Bumgardner GL, Melton L, Ducray PS, Banken L, Hall J, Boutouyrie BX. Equivalent pharmacokinetics of mycophenolate mofetil in African-American and Caucasian male and female stable renal allograft recipients. Am J Transplant 2003; 3: 1581–6.

40 van Gelder T, Smak Gregoor PJ, Weimar W. Drug interaction between mycophenolate mofetil and tacrolimus detectable within therapeutic mycophenolic acid monitoring in renal transplant patients. Ther Drug Monit 2000; 22: 639.

41 Hesselink DA, van Hest RM, Mathot RA, Bonthuis F, Weimar W, de Bruin RW, van Gelder T. Cyclosporine interacts with mycophenolic acid by inhibiting the multidrug resistance-associated protein 2. Am J Transplant 2005; 5: 987–94.

42 Kobayashi M, Saitoh H, Kobayashi M, Tadano K, Takahashi Y, Hirano T. Cyclosporin A, but not tacrolimus, inhibits the biliary excretion of mycophenolic acid glucuronide possibly mediated by multidrug resistance-associated protein 2 in rats. J Pharmacol Exp Ther 2004; 309: 1029–35.

43 Jiao Z, Zhong JY, Zhang M, Shi XJ, Yu YQ, Lu WY. Total and free mycophenolic acid and its 7-O-glucuronide metabolite in Chinese adult renal transplant patients: pharmacokinetics and application of limited sampling strategies. Eur J Clin Pharmacol 2007; 63: 27–37.

44 Liang MZ, Lu YP, Nan F, Yu Q, Qin YP, Zou YG. Pharmacokinetics of mycophenolic acid after a single and multiple oral doses of mycophenolate mofetil in Chinese renal transplant recipients. Transplant Proc 2004; 36: 2065–7.

45 Lu XY, Huang HF, Sheng-Tu JZ, Liu J. Pharmacokinetics of mycophenolic acid in Chinese kidney transplant patients. J Zhejiang Univ Sci B 2005; 6: 885–91.

46 Liang MZ, Lu YP, Nan F, Li YP. Pharmacokinetics of mycophenolic acid and its glucuronide after a single and multiple oral dose of mycophenolate mofetil in Chinese renal transplantation recipients. Transplant Proc 2006; 38: 2044–7.

47 Cho EK, Han DJ, Kim SC, Burckart GJ, Venkataramanan R, Oh JM. Pharmacokinetic study of mycophenolic acid in Korean kidney transplant patients. J Clin Pharmacol 2004; 44: 743–50.

48 van Hest RM, Mathot RA, Pescovitz MD, Gordon R, Mamelok RD, van Gelder T. Explaining variability in mycophenolic acid exposure to optimize mycophenolate mofetil dosing: a population pharmacokinetic meta-analysis of mycophenolic acid in renal transplant recipients. J Am Soc Nephrol 2006; 17: 871–80.

49 Arizon del Prado JM, Aumente MD, Lopez Granados A, Siles JR, Paulovic D, Romo E, Concha M, Vallés F, Casares J, Muñoz I, Segura C, Muñoz MI. Use of mycophenolate mofetil in patients with transplanted heart and renal insufficiency: the relevance of the pharmacokinetic study. Transplant Proc 2002; 34: 144–5.

50 Gonzalez-Roncero FM, Gentil MA, Brunet M, Algarra G, Pereira P, Cabello V, Peralvo M. Pharmacokinetics of mycophenolate mofetil in kidney transplant patients with renal insufficiency. Transplant Proc 2005; 37: 3749–51.

51 Meier-Kriesche HU, Shaw LM, Korecka M, Kaplan B. Pharmacokinetics of mycophenolic acid in renal insufficiency. Ther Drug Monit 2000; 22: 27–30.

52 Johnson HJ, Swan SK, Heim-Duthoy KL, Nicholls AJ, Tsina I, Tarnowski T. The pharmacokinetics of a single oral dose of mycophenolate mofetil in patients with varying degrees of renal function. Clin Pharmacol Ther 1998; 63: 512–8.

53 van Hest RM, van Gelder T, Bouw R, Goggin T, Gordon R, Mamelok RD, Mathot RA. Time-dependent clearance of mycophenolic acid in renal transplant recipients. Br J Clin Pharmacol 2007; 63: 741–52.

54 Atcheson BA, Taylor PJ, Kirkpatrick CM, Duffull SB, Mudge DW, Pillans PI, Johnson DW, Tett SE. Free mycophenolic acid should be monitored in renal transplant recipients with hypoalbuminemia. Ther Drug Monit 2004; 26: 284–6.

55 Picard N, Premaud A, Rousseau A, Le Meur Y, Marquet P. A comparison of the effect of ciclosporin and sirolimus on the pharmokinetics of mycophenolate in renal transplant patients. Br J Clin Pharmacol 2006; 62: 477–84.

56 Filler G, Zimmering M, Mai I. Pharmacokinetics of mycophenolate mofetil are influenced by concomitant immunosuppression. Pediatr Nephrol 2000; 14: 100–4.

57 Hubner GI, Eismann R, Sziegoleit W. Drug interaction between mycophenolate mofetil and tacrolimus detectable within therapeutic mycophenolic acid monitoring in renal transplant patients. Ther Drug Monit 1999; 21: 536–9.

58 Zucker K, Rosen A, Tsaroucha A, de Faria L, Roth D, Ciancio G, Esquenazi V, Burke G, Tzakis A, Miller J . Unexpected augmentation of mycophenolic acid pharmacokinetics in renal transplant patients receiving tacrolimus and mycophenolate mofetil in combination therapy, and analogous *in vitro* findings. Transpl Immunol 1997; 5: 225–32.

59 Levesque E, Delage R, Benoit-Biancamano MO, Caron P, Bernard O, Couture F, Guillemette C. The impact of UGT1A8, UGT1A9, and UGT2B7 genetic polymorphisms on the pharmacokinetic profile of mycophenolic acid after a single oral dose in healthy volunteers. Clin Pharmacol Ther 2007; 81: 392–400.

60 Sawyer MB, Innocenti F, Das S, Cheng C, Ramirez J, Pantle-Fisher FH, Wright C, Badner J, Pei D, Boyett JM, Cook E Jr, Ratain MJ. A pharmacogenetic study of uridine diphosphate-glucuronosyltransferase 2B7 in patients receiving morphine. Clin Pharmacol Ther 2003; 73: 566–74.

61 Miles KK, Stern ST, Smith PC, Kessler FK, Ali S, Ritter JK. An investigation of human and rat liver microsomal mycophenolic acid glucuronidation: evidence for a principal role of UGT1A enzymes and species differences in UGT1A specificity. Drug Metab Dispos 2005; 33: 1513–20.

62 Naesens M, Kuypers DR, Verbeke K, Vanrenterghem Y. Multidrug resistance protein 2 genetic polymorphisms influence mycophenolic acid exposure in renal allograft recipients. Transplantation 2006; 82: 1074–84.

63 Wada K, Takada M, Kotake T, Ochi H, Morishita H, Komamura K, Oda N, Mano A, Kato TS, Hanatani A, Nakatani T. Limited sampling strategy for mycophenolic acid in Japanese heart transplant recipients: comparison of cyclosporin and tacrolimus treatment. Circ J 2007; 71: 1022–8.